

**Late Miocene-Pliocene climate evolution recorded by the red clay covered  
on the Xiaoshuizi planation surface, NE Tibetan Plateau**

Xiaomiao Li<sup>1</sup>, Tingjiang Peng<sup>1</sup>, Zenhua Ma<sup>1</sup>, Meng Li<sup>1</sup>, Zhantao Feng<sup>1</sup>, Benhong Guo<sup>1</sup>, Hao Yu<sup>1</sup>, Xiyan  
Ye<sup>1</sup>, Zhengchuang Hui<sup>1</sup>, Chunhui Song<sup>2</sup>, Jijun Li<sup>1,3</sup>

1. MOE Key Laboratory of Western China's Environmental Systems, College of Earth and Environmental  
Sciences, Lanzhou University, Lanzhou 730000, China

2. School of Earth Sciences, Key Laboratory of Western China's Mineral Resources of Gansu Province,  
Lanzhou University, Lanzhou 730000, China

3. College of Geography Science, Nanjing Normal University, Nanjing 210023, China

---

\*Corresponding author: Key Laboratory of Western China's Environmental Systems  
(Ministry of Education), College of Earth and Environmental Science, Lanzhou University,  
Lanzhou 730000, China; *E-mail address*: [lijj@lzu.edu.cn](mailto:lijj@lzu.edu.cn) (J.J. Li), *Fax*: +86-931-891-2724;  
*Tel.*: +86-931-891-2724

## 23    **Abstract**

24           The Pliocene climate and its driving mechanisms have attracted substantial scientific  
25   interest because of its potential as an analog for near-future climates. The late Miocene-  
26   Pliocene red clay sequence of the main Chinese Loess Plateau (CLP) has been widely used to  
27   reconstruct the history of interior Asian aridification and Asian monsoon. However, red clay  
28   sequences deposited on the planation surface of the Tibetan Plateau (TP) are rare. A  
29   continuous red clay sequence was recently discovered on the uplifted Xiaoshuizi (XSZ)  
30   planation surface in the Maxian Mountains, northeastern (NE) TP. In this study, we analyzed  
31   multiple climatic proxies from the XSZ red clay sequence to reconstruct the late Miocene-  
32   early Pliocene climate history of the NE TP and to assess regional climatic differences  
33   between the central and western CLP. Our results demonstrate the occurrence of minimal  
34   weathering and pedogenesis during 6.7-4.8 Ma, which indicates that the climate was arid. We  
35   speculate that precipitation delivered by the palaeo- East Asian Summer Monsoon (EASM)  
36   was limited during this period, and that the intensification of the westerlies circulation  
37   resulted in arid conditions in the study region. Subsequently, enhanced weathering and  
38   pedogenesis occurred during 4.8-3.6 Ma, which attests to an increase in effective moisture.  
39   We ascribe the arid-humid climatic transition near 4.8 Ma to the expansion of the palaeo-  
40   EASM. Increasing Arctic temperatures, the poleward expansion of the tropical warm pool  
41   into subtropical regions and the freshening of the subtropical Pacific in response to the  
42   closure of the Panamanian Seaway may have been responsible for the thermodynamical  
43   enhancement of the palaeo-EASM system, which permitted more moisture to be transported  
44   to the NE TP.

**Keywords:** Late Miocene-Pliocene; Xiaoshuizi Planation surface; Red Clay; Palaeo-EASM; Westerly Circulation

## 1. Introduction

The Pliocene, including the Zanclean (5.33-3.60 Ma) and Piacenzian (3.60-2.58 Ma) stages, is one of the most intensively studied intervals of the pre-Quaternary on climate change research. The Zanclean climate was generally warm-wet and often used as an analogue for near-future climate conditions in terms of carbon dioxide levels ranging from 280-415 ppm ([Tripathi et al., 2009](#); [Pagani et al., 2010](#)), and comparable temperatures in the tropic region ([Herbert et al., 2010, 2016](#)). On the other hand, the Zanclean is markedly different from today and several critical changes in thermohaline and atmospheric circulation towards modern conditions were occurring ([Haug et al., 2005](#); [Lawrence et al., 2006](#); [Chaisson and Ravelo, 2000](#)). For example, the early-Pliocene global mean temperature was approximately 4 °C warmer ([Brierley and Fedorov, 2010](#)) and the sea levels estimated to have been ~25 m higher than today ([Dowsett et al., 2010](#)). Temperatures at high northern latitudes were considerably higher and therefore continental glaciers were almost absent from the Northern Hemisphere ([Ballantyne et al., 2010](#); [Dowsett et al., 2010](#)). The zonal and meridional sea surface temperature gradients in the Northern Hemisphere was weak and gradually changed toward a modern much more pronounced spatial temperature contrasts ([Fedorov et al., 2013](#); [Brierley et al., 2009, 2010](#)). The low meridional surface temperature gradient resulted in weaker meridional circulation during this interval ([Fedorov](#)

et al., 2013; Brierley et al., 2009) and low east-west sea surface temperature gradient in the tropical Pacific during this interval is believed to have given rise to a permanent El Nino Southern Oscillation (Lawrence et al., 2006). However, whether permanent El Nino-like conditions were sustained during the Pliocene is still controversial (Wara et al., 2005; Watanabe et al., 2011; Zhang et al., 2014). Meanwhile, the episodic uplift of the TP (Li et al., 2015; Zheng et al., 2000; Fang et al., 2005a, 2005b) and gradual closing of the Panama seaway (Keigwin et al., 1978; O'Dea et al., 2016) were underway. The former substantially influenced the palaeoclimate change (An et al., 2001; Ding et al., 2001; Liu et al., 2014) and the later resulted in reorganization of the global thermohaline circulation (Haug et al., 1998, 2001). Together these observations imply a structural change in global climate from the early Pliocene to present. We have to ask what the regional climate like under such special climatic and tectonic settings.

East Asia is one of the key regions for studying the aridification of the Asian interior and the Asian monsoon evolution which is tightly linked to the uplift of the TP, the regional climate change and global temperature and ice volume evolution (An et al., 2001; Ding et al., 2001; Li et al., 2008; Clift et al., 2008; Nie et al., 2014; Ao et al., 2016; Sun et al., 2006a, 2017; Chang et al., 2013; Liu et al., 2014). Previous research has revealed that the red clay was widely deposited since the late Miocene across the CLP, indicating that the Asian aridification related to the uplift of the TP enhanced (Guo et al., 2001; Song et al., 2007; An et al., 2014; Ao et al., 2016; Li et al., 2017). In the eastern and central CLP where climate is dominated by East Asian Monsoon, palaeontological evidence, mineral magnetic parameters and geochemical records from the red clay indicate dry climatic conditions

during the late Miocene but generally wet climatic conditions during the early Pliocene (Wang et al., 2006; Guo et al., 2001; Wu et al., 2006; Song et al., 2007; Sun et al., 2010; An et al., 2014; Ao et al., 2016). The most controversial climatic change occurred during the interval from 4.8-4.1 Ma, for which climate reconstructions from different proxies indicate conflicting palaeo-environmental trends. For example, field observations and pollen records indicate an intensified summer monsoon intensity, but low magnetic susceptibility values are more consistent with arid rather than wet climatic conditions (Ding et al., 2001; Ma et al., 2005; Song et al., 2007; Sun et al., 2010). It is thought that waterlogging and iron reduction resulting from high precipitation significantly affected the climatic significance of magnetic susceptibility records during this period (Ding et al., 2001). In addition to the East Asian Monsoon, the westerlies also had an impact on climate of East Asia. However, patterns of climate change in westerlies dominated regions were different from the eastern and central CLP during the early Pliocene. Geochemical, stratigraphic and pollen evidence from the Qaidam and Tarim basins has demonstrated that aridification had intensified since the early Pliocene (Fang et al., 2008; Sun et al., 2006a, 2017; Chang et al., 2013; Liu et al., 2014). Although the general climatic trends of the main CLP and northern TP during this period were well recorded, palaeoclimatic change in the NE TP which is at the junction of the westerlies and monsoonal influences remains unclear. Therefore, determining the climatic conditions of the NE TP during the early Pliocene not only improves our understanding of the regional climate change, but also provides insights into the responses of the palaeo-EASM and westerlies to TP uplift and changes in the global climate system at this time.

Continuous red clay sequence was recently discovered on the uplifted XSZ planation surface in the NE TP and has been dated via high-resolution magnetostratigraphy analysis (Li et al., 2017). The distinctive geomorphological and climatic characteristics of the XSZ red clay sequence differentiates it from the main CLP red clay, and provides the opportunity to reveal the late Miocene-early Pliocene climate history of the NE TP and to discuss the climatic differences between the central and western CLP. In this study, we measured multiple climatic proxies from the late Miocene-Pliocene XSZ red clay core and then the detailed history of precipitation, chemical weathering and pedogenesis during 6.7-3.6 Ma are reconstructed. Finally, the regional climate evolution and its possible mechanisms have been further discussed.

## **2. Regional background**

The XSZ planation surface is located in Yuzhong County in the western Chinese Loess Plateau (Fig. 1). The main XSZ planation surface is at an altitude of 2800 m in Maxian mountains where it has truncated Precambrian gneiss. The Maxianshan are rejuvenated mountains which protrude into the broad Longzhong Basin, and are in a climatically sensitive zone because of the combined influences of the Asian Monsoon and the northern branch of the mid-latitude westerly circulation system. The planation surface is mantled by over 30 m of loess and over 40 m of red clay. Our previous bio-magnetostratigraphic study has demonstrated that the red clay sequence covering the XSZ planation surface is dated to ~6.9-3.6 Ma (Li et al., 2017). Here, we use the XSZ drill core to reconstruct and discuss the regional climate during the Miocene-Pliocene. The long, continuous well-dated record of the

drill core is superior to that of the Shangyaotan core mentioned in Li et al. (2017). Yuzhong County lies within the semi-arid temperate climate zone at the junction of the eastern monsoon area, the arid area of northwest China, and the TP cold region. The mean annual temperature during 1986-2016 was ~7.0 °C and the annual precipitation was 260-550 mm. Most (80%) of the precipitation is in summer and autumn. The data were obtained from the National Meteorological Information Center (<http://data.cma.cn/>) of the Chinese Meteorological Administration (MCA). The spatial distribution of precipitation is uneven, decreasing from south to north in Yuzhong County. Precipitation amount increases with elevation at a rate of 27 mm per 100 m, attaining a maximum of 800 mm at the top of Maxianshan.

### 3. Material and methods

The XSZ core (35.81154 °N, 103.8623 °E and 2758.1 m above sea level) is composed of 42 m of pure red clay and ~3 m of red clay with an increasing angular gravel content at the base (Fig. 1 b). The red clay is composed of brownish red and yellowish clay layers (Fig. 2). The upper 20 m contains numerous horizontal carbonate nodule horizons and most of these horizons underline the brownish red layer. There are also occasional carbonized plant root channels, elliptical worm burrows and fossil snail shell fragments. Fe-Mn stains are more frequent in the brownish layers than in the yellowish layers, which is also the case for the carbonized root channels. The red clay across the XSZ planation surface is similar to that of typical eolian red clay in the CLP; both are characterized by numerous carbonate nodule-rich horizons (Fig. 2 b).

Samples for grain-size, carbonate content and magnetic susceptibility measurements were taken at 5-cm intervals, and samples for geochemical analysis were collected at 25-cm intervals. The grain-size distribution of samples was measured with a Malvern Mastersizer 2000 with a detection range of 0.02-2000  $\mu\text{m}$ . Magnetic susceptibility was measured using a Bartington MS2 meter and MS2B dual-frequency sensor at two frequencies (470 Hz and 4700 Hz, designated  $\chi_{\text{lf}}$  and  $\chi_{\text{hf}}$ , respectively). Three measurements were made at each frequency and the final results were averaged. The frequency-dependent magnetic susceptibility ( $\chi_{\text{fd}}$ ) was calculated as  $\chi_{\text{lf}} - \chi_{\text{hf}}$ . Chemical composition was measured via X-ray fluorescence using a Panalytical Magix PW2403. The sample preparation procedure for XRF analysis was as follows: Bulk samples were heated to 35°C for 7 days and then ground to less than 75 $\mu\text{m}$  using an agate mortar; finally, ~4 g of powdered sample was pressed into a pellet with a borate coating using a semiautomatic oil-hydraulic laboratory press (model YYJ-40). All the measurements were conducted at the MOE Key Laboratory of Western China's Environmental Systems, Lanzhou University.

Silicate-bound CaO (CaO\*) can be estimated, in principle, by the equation:  $\text{CaO}^*(\text{mol}) = \text{CaO}(\text{mol}) - \text{CO}_2(\text{calcite mol}) - 0.5 \text{CO}_2(\text{dolomite mol}) - 10/3 \text{P}_2\text{O}_5(\text{apatite mol})$  (Fedo et al., 1995). It is generally calculated based on the assumption that all the  $\text{P}_2\text{O}_5$  is associated with apatite and all the inorganic carbon is associated with carbonates. Thus, the CaO\* of the XSZ red clay was calculated using the following equivalent equation:

$$\text{CaO}^*(\text{mol}) = \text{CaO}(\text{mol}) - \text{CaCO}_3(\text{mol}) - \frac{10}{3} * \frac{\text{P}_2\text{O}_5}{M(\text{P}_2\text{O}_5)}$$

The carbonate content was measured with a calcimeter using the volumetric method of Avery and Bascomb (1974) in the Key Laboratory of Mineral Resources in Western China



(Gansu Province), Lanzhou University.

We use the coefficient of variation (CV) to measure the variability of the records. The higher the CV, the more variable the record. The CV is defined as:

$$CV = 100 * \frac{\text{Standard deviation}}{\text{Mean}}$$

Each sample age was estimated using linear interpolation to derive absolute ages, constrained by our previous magnetostratigraphic study (Fig. 1). The average temporal resolution of the records is 3.8 kyr. Some 80 % of the sequence has a sampling resolution of 4 kyr or less.

#### 4. Results

Profiles of the various proxies are illustrated in Figure 3 and there is an obvious difference in the character of the fluctuations above and below the depth of 16.5 m (~ 4.8 Ma). Above 16.5 m, the carbonate content fluctuates at a lower level but with greater amplitude accompanied by the noted increase in nodule horizons underlying leached zones in the field, and the magnetic susceptibility also fluctuates at greater amplitude. In addition, the CV of most of the records is greater above the boundary than below (Table 1). This suggests that the climate became more humid and variable after 4.8 Ma. Meanwhile, a noticeable drop in deposition rate around 4.8 Ma occurred (Li et al., 2017). Thus, the red clay sequence was divided into two intervals: *Interval I* (6.7-4.8 Ma) and *Interval II* (4.8-3.6 Ma). The characteristics of the individual proxy records are described in detail below.

## **Carbonate content**

During *Interval I*, the carbonate content fluctuates from 3.8-39.2% and has a high average value (17.4%); the carbonate content contrast between leach layers and accumulation layers is generally low and the carbonate content decreases upwards (Fig. 3). From 29-16.5 m, the fluctuations are of greater amplitude than during 42-29 m. During *Interval II*, the carbonate content fluctuations have a large amplitude (from 1.6-39.1%) but a low average value (13.8%). From 16.5-4.5 m there are several leaching-accumulation layers, with <7% carbonate content in the leached layers and >20% carbonate content in the accumulation layers.

## **Element geochemistry**

The XSZ red clay consists mainly of SiO<sub>2</sub>, Al<sub>2</sub>O<sub>3</sub>, CaO and Fe<sub>2</sub>O<sub>3</sub> with low concentrations (<5%) of MgO, K<sub>2</sub>O, Na<sub>2</sub>O, Sr, Rb and Ba (Table 1). During *Interval I*, K<sub>2</sub>O ranges from 1.9-3.3% with an average content of 2.6%. Na<sub>2</sub>O ranges from 0.14-1.52% with an average content of 1.2%. Rb ranges from 80-125 ppm with an average content of 103.9 ppm. Sr ranges from 150-252 ppm with an average content of 211.7 ppm. During *Interval II*, K<sub>2</sub>O ranges from 2-3.7% with an average content of 3%. Na<sub>2</sub>O ranges from 0.94-1.54 % with an average content of 1.23%. Rb ranges from 74-134 ppm with an average content of 109.9 ppm. Sr ranges from 141-281 ppm with an average content of 214.6 ppm. The variations in CaO show the same trend as carbonate content. The variations of Rb and K<sub>2</sub>O are synchronous and roughly opposite to that of CaO. The changes of Sr show some similarity with magnetic susceptibility before 4.8 Ma but with CaO after 4.8 Ma. Accordingly, table 2 indicates CaO shows positive correlation with CaCO<sub>3</sub> and Sr, while negative correlation with

other elements. The variations in CaO, K<sub>2</sub>O, Sr and Rb content during 4.8-3.6 Ma are greater than those during 6.7-4.8 Ma, which is also indicated by the CV of these elements (Table 1).

### **Magnetic susceptibility**

Magnetic susceptibility also shows pronounced differences between the two intervals (Fig. 3). During *Interval I*,  $\chi_{hf}$  ranges from  $9.6-33.3 \times 10^{-8} \text{ m}^3/\text{kg}$  with an average of  $19.4 \times 10^{-8} \text{ m}^3/\text{kg}$ ;  $\chi_{lf}$  ranges from  $11.4-36.1 \times 10^{-8} \text{ m}^3/\text{kg}$  with an average of  $20.3 \times 10^{-8} \text{ m}^3/\text{kg}$ ; and  $\chi_{fd}$  ranges from  $0-2.8 \times 10^{-8} \text{ m}^3/\text{kg}$  with an average of  $1.0 \times 10^{-8} \text{ m}^3/\text{kg}$ . During *Interval II*,  $\chi_{hf}$  ranges from  $12.8-53.9 \times 10^{-8} \text{ m}^3/\text{kg}$  with an average of  $25.4 \times 10^{-8} \text{ m}^3/\text{kg}$ ;  $\chi_{lf}$  ranges from  $13.6-59.0 \times 10^{-8} \text{ m}^3/\text{kg}$  with an average of  $26.9 \times 10^{-8} \text{ m}^3/\text{kg}$ ; and  $\chi_{fd}$  ranges from  $0-4.7 \times 10^{-8} \text{ m}^3/\text{kg}$  with an average of  $1.2 \times 10^{-8} \text{ m}^3/\text{kg}$ . Clearly, the average values of the three parameters are higher during *Interval II* than during *Interval I*. The amplitudes of the fluctuations in the three parameters during *Interval II* are also larger than those during *Interval I*. From 16-15 m, 13-11 m and 7-5 m, the values of the three parameters are high.

### **Grain size**

The average clay content ( $<2 \mu\text{m}$ ) is 8.2% during *Interval I* and 8.0% during *Interval II*. The fluctuations in clay content are minor, except for maxima at about 15m, 12m and 6m (Fig. 3). The coarse silt component ( $>40 \mu\text{m}$ ), mainly carried by the East Asian winter monsoon, exhibits a different trend to that of the clay content, as well as to other proxies described above. From 6.7-4.8 Ma, the variation of the  $>40 \mu\text{m}$  fraction is characterized by low values and high-frequency fluctuations, whereas after 4.8 Ma it exhibits high values and lower frequency fluctuations.

## **5. Discussion**

## 5.1 Palaeoenvironmental interpretation of the proxies

The carbonate content of aeolian sediments is sensitive to changing climatic conditions, and can be readily remobilized and deposited in responses to changes in precipitation and evaporation intensity. Previous studies demonstrated that carbonate in the loess-red clay sequences of the CLP varies with precipitation (Fang et al., 1999; Sun et al., 2010). The carbonate is mainly derived from a mixture of airborne dusts (Fang et al., 1999). Soil micromorphological evidence from the Lanzhou loess demonstrates that the carbonate grains in loess are little altered, whereas those in the palaeosols have undergone a reduction in size as a result of leaching and reprecipitation in the lower Bk horizons as secondary carbonate (Fang et al., 1994, 1999). Furthermore, seasonal alternations between wet and dry conditions are thought to be a key factor in driving carbonate dissolution and reprecipitation (Sun et al., 2010). Thus, changes in carbonate content are generally controlled by the effective precipitation. When effective precipitation is high, carbonate leaching increases, and vice versa. Thus, the carbonate content is regarded as an effective precipitation proxy for characterizing wet-dry oscillations as well as summer monsoon evolution (Fang et al., 1999; Sun et al., 2010).

Chemical weathering intensity is generally evaluated by the ratio of mobile (e.g. K, Ca, Sr and Na) to non-mobile elements (e.g. Al and Rb). In general, Sr shows analogous geochemical behavior to Ca and is easily released into solution and mobilized in the course of weathering, whereas Rb is relatively immobile under moderate weathering conditions due to its strong adsorption to clay minerals (Nesbitt et al., 1980; Liu et al., 1993). Thus, the Rb/Sr ratio potentially reflects chemical weathering intensity. However, Sr may substitute for Ca in

carbonates, which may limit the environmental significance of the Rb/Sr ratio ([Chang et al., 2013](#); [Buggle et al., 2011](#)). The correlation between Sr and CaO\* (silicate CaO) is significant at the 99% confidence interval, while the correlation between Sr and CaCO<sub>3</sub> is not significant. This means that the variation of Sr is determined by weathering intensity. Thus, we speculate that in our samples the Rb/Sr ratio mainly reflects the weathering intensity (Fig. 4 d and e). In addition, the K<sub>2</sub>O/Na<sub>2</sub>O ratio is used to evaluate the secondary clay content in loess and is also a measure of plagioclase weathering, avoiding biases due to uncertainties in separating carbonate Ca from silicate Ca ([Liu et al., 1993](#); [Buggle et al., 2011](#)). Na<sub>2</sub>O is mainly produced by plagioclase weathering and is easily lost during leaching as precipitation increases. By contrast, K<sub>2</sub>O (mainly produced by the weathering of potash feldspar) is easily leached from primary minerals and is then absorbed by secondary clay minerals with ongoing weathering ([Yang et al., 2006](#); [Liang et al., 2013](#)). In the arid and semi-arid regions of Asia, K<sub>2</sub>O is enriched in palaeosols compared to loess horizons ([Yang et al., 2006](#)). Thus, high K<sub>2</sub>O/Na<sub>2</sub>O ratios are indicative of intense chemical weathering.

In the red clay-loess sequence of the CLP, magnetic parameters and the clay (<2 μm) content are well correlated and thus are regarded as the proxies of EASM strength ([Liu et al., 2004](#)). Aeolian particles usually have two distinct magnetic components, consisting of detrital and pedogenic material ([Liu et al., 2004](#)).  $\chi_{\text{f}}$  can reflect the combined susceptibility of both components, but changes in  $\chi_{\text{f}}$  are dominantly affected by changes in the concentration of pedogenic grains ([Liu et al., 2004](#)). The grain-size distribution of pedogenic particles within the superparamagnetic (SP) to single-domain (SD) size range has been shown to be constant ([Liu et al., 2004, 2005](#)). Thus,  $\chi_{\text{fd}}$  can be used to detect superparamagnetic minerals produced by

pedogenesis and therefore the correlation coefficient between  $\chi_{lf}$  and  $\chi_{fd}$  is a measure of the contribution of SP grains ( $<0.03 \mu\text{m}$  for magnetite) to the bulk susceptibility (Liu et al., 2004; Xia et al., 2014). As shown in Figure 4a,  $\chi_{lf}$  is positively correlated with  $\chi_{fd}$ , which means that the magnetic susceptibility of the XSZ red clay mainly reflects pedogenic enhancement of the primary aeolian ferromagnetic content through the in-situ formation of fine-grained ferrimagnetic material. This means that the magnetic susceptibility primarily reflects pedogenic intensity. Both the original and pedogenic magnetic signals can be separated using a simple linear regression method (Liu et al., 2004; Xia et al., 2014), which we use to extract the lithogenic ( $\chi_0$ ) and pedogenic magnetite/maghemite ( $\chi_{pedo}$ ) components. In this study, pedogenic magnetite/maghemite accounts for 11% of the susceptibility ( $\chi_{pedo} = \chi_{fd} / 0.11$ ).

Pedogenesis results in enhanced secondary clay formation (Sun and Huang, 2006b); however, not all of the clay particles are derived from in situ pedogenesis, but rather are inherited from aeolian transport and deposition. Clay particles can adhere to coarser silt and sand particles (Sun and Huang, 2006b). In the western CLP, the coarse silt ( $>40 \mu\text{m}$ ) content is regarded as a rough proxy for winter monsoon strength (Wang et al., 2002). Therefore, to eliminate this signal from the primary clay particles, the  $<2 \mu\text{m}/>40 \mu\text{m}$  ratio can be used to evaluate pedogenic intensity. Furthermore, the similarity of the variations of  $<2 \mu\text{m}/>40 \mu\text{m}$  ratio and  $\chi_{pedo}$  confirms that both proxies are sensitive to pedogenic intensity in the XSZ red clay (Fig. 6).

## 5.2 Time- and frequency- domain analysis of carbonate content and $\chi_{pedo}$

Power spectral analyses of carbonate content and  $\chi_{pedo}$  show different dominant cycles (Fig. 5). In detail,  $\chi_{pedo}$  is concentrated in the eccentricity (100 kyr), obliquity (41 kyr) and

precession (21 kyr) bands and another periodicities (71 kyr and 27 kyr) are also evident. In contrast, the carbonate signal is concentrated in the precession (21 kyr) and obliquity (41 kyr) bands, but it also exhibits even more prominent periodicities at 56 kyr and 30 kyr. Furthermore, the fluctuations in  $\text{CaCO}_3$ , weathering and pedogenesis indices agree well with orbital eccentricity variations during 4.8-3.9 Ma (Fig. 5). Three orbital periodic signals were also detected in the other sites of the CLP from late Miocene to early Pliocene, which means changes of orbital parameters really had impact on climate of the CLP (Han et al., 2011).

King (1996) proposed that non-orbital cycles may possibly originate from harmonics or interactions of the orbital cycles, while Lu (2004) ascribed them to unstable dust depositional processes followed by varying degrees of pedogenesis in palaeosol units. In the XSZ section, deposition rate was low and uneven, which potentially resulted in the incomplete preservation of the paleoclimatic signal, especially for short precession cycles. Meanwhile, pedogenic and post-depositional compaction would also weaken the orbital signals and produce spurious cycles. In addition, the carbonate content at various depths is affected by leaching which means that the record integrates soil polygenetic processes, thus obscuring orbital forcing trends related to precipitation amount. Therefore, we speculate that uneven and low deposition rates combined with compaction and leaching processes may weaken the orbital signals and be responsible for presence of non-orbital cycles in XSZ section.

To investigate the post-6.7 Ma evolution of the climate signals in the XSZ section in the frequency domain, we filtered the carbonate content and  $\chi_{\text{pedo}}$  time series at the 100, 41, and 21-kyr periods, using Gaussian band filters centered at frequencies of 0.01, 0.02439, and 0.04762 respectively, and compared them with the equivalent filtered components of the

stacked deep-sea benthic oxygen isotope record. The results show that the fluctuations of the three filtered components (especially the 41-kyr component) of both proxies changes from a low amplitude during 6.7-4.8 Ma to a relatively high amplitude during 4.8-3.9 Ma (Fig. 5). The enhanced orbital-scale variability of the two proxies from 4.8-3.9 Ma implies increased seasonality and wet-dry contrasts. This shift is not observed in the Earth orbital parameters but is observed in the filtered 41-kyr component of the stacked deep-sea benthic oxygen isotope record ( $\delta^{18}\text{O}$ ). This may mean that the enhancement for wet-dry contrast at the XSZ site was not driven directly by changes in solar radiation intensity but rather was linked with changes in ice volume or global temperature.

### **5.3 Late Miocene-Pliocene climate history revealed by the Xiaoshuizi red clay**

#### **5.3.1 Multi proxy evidence for a dry climate during 6.7-4.8 Ma**

We used the aforementioned proxies of pedogenesis and chemical weathering to reconstruct the late Miocene and early Pliocene climatic history of the Xiaoshuizi planation surface. As shown in Figure 6 and Table 3, there is a significant change in most of the proxies (carbonate, Rb/Sr,  $\text{K}_2\text{O}/\text{Na}_2\text{O}$  and  $\chi_{\text{pedo}}$ ) near 4.8-4.7 Ma, and therefore the climatic record can be divided into two intervals. During interval I (6.7-4.8 Ma), the relatively high carbonate values with minor fluctuations indicate that the climate was dry, and low Rb/Sr and  $\text{K}_2\text{O}/\text{Na}_2\text{O}$  ratios also support the occurrence of weak chemical weathering. Notably, both the Rb/Sr and  $\text{K}_2\text{O}/\text{Na}_2\text{O}$  ratios show opposite trends to carbonate content, meaning that low effective precipitation resulted in weak chemical weathering. Furthermore, the pedogenic proxies ( $<2\ \mu\text{m}/>40\ \mu\text{m}$  ratio,  $\chi_{\text{pedo}}$  and  $\chi_{\text{lf}}$ ) characterised by low values with minor fluctuations, generally support the occurrence of weak pedogenesis under an arid climate.



Thus, the climate at the XSZ site during this interval was relatively arid, characterized by weak chemical weathering and pedogenic intensity. However, subtle differences exist between the carbonate and pedogenic indexes. It is evident that the carbonate content decreases with increased variation amplitude after 5.5 Ma, which is consistent with the cycles of carbonate nodules within paleosol horizons observed in the field (Li et al., 2017). It is possible that increased precipitation since 5.5 Ma induced eluviation-redeposition of carbonate. However, the pedogenic indexes indicate that the generally arid climate was interrupted by two episodes of enhanced pedogenesis, at 5.85-5.7 Ma and 5.5-5.35 Ma. The subtle differences may result from differences in the sensitivity of magnetic susceptibility and carbonate content to precipitation variability when precipitation is low (Sun et al., 2010). In addition, a coeval mollusk record from the western Liupanshan showed that cold-aridiphilous species dominated, which also indicates that cold and dry climatic conditions occurred in the western CLP during the late Miocene (Fig. 7 g).

Coeval pollen, mollusk and magnetic records from the central and eastern CLP also indicate generally dry and cold climatic conditions (Wang et al., 2006; Wu et al., 2006; Nie et al., 2014). However, the principal difference is that at XSZ the arid climate was relatively stable, while the climate of the central and eastern CLP was interrupted by several humid stages. For example, two humid stages (at 6.2-5.8 Ma and 5.4-4.9 Ma) are recorded by the magnetic susceptibility of red clay in the central and eastern CLP, but are absent in the magnetic susceptibility record from XSZ (Fig. 7). Notably, the 41-kyr filtered component of thermo-humidiphilous species from Dongwan was damped in the late Miocene (Li et al., 2008). Similarly, the amplitude of the orbital periodicities, filtered from the XSZ carbonate

content and  $\chi_{\text{pedo}}$  records, was obviously damped during 6.7-4.8 Ma. However, the three periodicities in the Summer Monsoon index from the central CLP show no obvious difference between the late Miocene and Pliocene, but only a slight reduction in variability after 4.2 Ma (Sun et al., 2010). Therefore, we agree that a dry climate prevailed on the CLP during the interval of 6.7-4.8 Ma. However, the only difference was that the climate in the central and eastern CLP fluctuated more substantially than was the case in the vicinity of the XSZ red clay section.

The especially damped response of the wet-dry climatic oscillations in the western CLP to obliquity forcing may indicate that the palaeo-EASM had a negligible influence in the western CLP. It is widely known that the summer monsoon intensity decreases from southeast to northwest across the CLP. A regional climate model experiment demonstrated that the modern East Asian Summer Monsoon was not fully established in the late Miocene and had only a small impact on northern China (Tang et al., 2011). A weak palaeo-EASM intensity from 7.0-4.8 Ma was revealed by hematite/goethite and smectite/kaolinite ratios at ODP Site 1148 in the South China Sea (SCS) (Fig. 7 i and j). Therefore, we infer that the palaeo-EASM was weak and had only a minor impact on the climate in the study region. In addition, previous studies indicated that the red clay may have been transported by both low-level northerly winds and upper-level westerlies (Sun et al., 2004; Vandenberghe et al., 2004) and thus the impact of the westerly circulation on the study region cannot be ignored. Notably, the variation of the pedogenic proxies roughly parallels to that of the stacked deep-sea benthic foraminiferal oxygen isotope curve (Fig. 6), that  $\chi_{\text{pedo}}$  shows a significant positive relationship with  $\delta^{18}\text{O}$  at 80 % confidence interval (Fig. 4 f). It indicates when global

temperature was low, pedogenic intensity increased. It is unreasonable to conclude that precipitation in the study area was dominated by the palaeo-EASM and thus we speculate that from 6.7-4.8 Ma precipitation transported by the palaeo-EASM was limited and the westerly circulation probably dominated the regional climate.

The simultaneous reduction in amplitude of the 41-kyr filtered components from the western CLP and the deep sea  $\delta^{18}\text{O}$  record from 6.7-4.8 Ma likely indicates that the dry climate was related to changes in global temperature and ice volume. A sustained cooling occurred in both hemispheres during the late Miocene and the cooling culminated between 7 and 5.4 Ma (Herbert et al., 2016).  $\delta^{18}\text{O}$  records from DSDP and ODP sites show an increase of  $\sim 1.0\text{‰}$  during the late Miocene which resulted from the increased ice volume and the associated decrease in global temperature (Zachos et al., 2001). In the Northern Hemisphere, transient glaciations appeared when the cooling culminated (Herbert et al., 2016). Records from high latitude regions of the Northern Hemisphere indicate continuously decreasing temperatures and increasing ice volume during the late Miocene (Jansen and Sjøholm, 1991; Mudie and Helgason, 1983; Haug et al., 2005). During the Quaternary, a dry climate prevailed during glacial periods when global average temperature (especially in summer) was low. Cool summers could result in a small land-sea thermal contrast which in turn weakened the palaeo-EASM. Furthermore, the increased ice volume in the Northern Hemisphere resulted in an increased meridional temperature gradient (Herbert et al., 2016), thus strengthening the westerlies and driving them southward. This would have prevented the northwestward penetration of the Asian Summer Monsoon, which is also proposed as the driving mechanism for a weak EASM in northern China during glacial periods (Sun et al.,

2015). Thus, the southward shift of the westerlies had a significant impact on the XSZ region. However, moisture sources for the westerly flow are distant from the CLP (Nie et al., 2014), and only a relatively small amount of moisture was carried to the CLP, resulting in a dry and stable climate in the XSZ region. In conclusion, global cooling and increasing ice volume in the Northern Hemisphere contributed to the dry climatic conditions in the study region.

### **5.3.2 Humid climate with pronounced fluctuations during 4.8-3.6 Ma**

During interval II (4.8-3.6 Ma), the proxy evidence indicates that the previously arid climate of the XSZ area became humid. The carbonate content was low on average but with large fluctuations, indicating that the climate was generally humid with increased dry-wet oscillations, especially during 4.8-3.9 Ma. Several eluvial-illuvial cycles are evident during 4.8-3.9 Ma; the carbonate content in the eluvial horizons was less than 7%, whereas in illuvial horizons it exceeded 20% (Fig. 6). Research on migration process of carbonate indicated seasonally wet/dry climate is a key factor in driving carbonate dissolution and reprecipitation, and strong seasonally biased precipitation enhances the leaching process and produces thick leached horizons (Rossinsky and Swart, 1993; Zhao, 1995, 1998). The emergence of high-frequency cycles of carbonate eluviation-redeposition indicates that seasonal precipitation increased during this interval. Furthermore, the variations of Rb/Sr and  $K_2O/Na_2O$  ratios are very similar to those of carbonate content, which suggests that weathering intensity was related to precipitation amount. Generally, high  $<2\ \mu m / >40\ \mu m$  ratio,  $\chi_{pedo}$  and  $\chi_{lf}$  correspond to large contrasts in carbonate content between eluvial and illuvial horizons; thus, increased precipitation had a significant influence on pedogenic intensity. High precipitation persisted from 4.8-3.9 Ma and weathering and pedogenic

intensity were strong. From 4.60-4.25 Ma, pedogenesis and weathering intensity reached a maximum, as did precipitation intensity, which is manifested by the enhanced eluviation and carbonate accumulation. During 3.9-3.6 Ma, precipitation decreased, and weathering and pedogenic intensity also weakened. Consistent with the records of the XSZ section, mollusk records from Dongwan also indicate the occurrence of warm and humid conditions in the western CLP during the early Pliocene (Fig. 7 h).

Palynological and terrestrial mollusk records from the central CLP also indicate relatively humid conditions during the early Pliocene (Wang et al., 2006; Wu et al., 2006). Magnetic susceptibility records from the central and eastern CLP are similar to that from the XSZ section in that both the magnitude and the variability are high during 4.8-3.6 Ma. From 4.1-3.9 Ma, the increased magnetic susceptibility indicates that humid climatic conditions prevailed across the entire CLP (Fig. 7). Evidently, when precipitation amount peaked during 4.60-4.25 Ma in the vicinity of the XSZ section, the magnetic susceptibility values at Xifeng, Lingtai and Chaona were low. However, a record of  $\text{Fe}_2\text{O}_3$  ratio from Lingtai reveals extremely high values, corresponding to the presence of abundant clay coatings, during 4.8-4.1 Ma and this interval was interpreted as experiencing the strongest EASM intensity in the CLP since 7.0 Ma (Ding et al., 2001). In addition, the relative intensity of pedogenic alteration of the grain-size distribution was the strongest during the interval from 4.8-4.2 Ma in the Lingtai section (Sun et al., 2006c). Pollen assemblages at Chaona indicate a substantially warmer and more humid climate from 4.61-4.07 Ma (Ma et al., 2005). These various lines of evidence indicate that during 4.60- 4.25 Ma the climate was warm and humid in the central CLP. Gleying has been implicated in reducing the value of magnetic

susceptibility as a record of precipitation during this period (Ding et al., 2001). When soil moisture regularly exceeds the critical value, dissolution of ferrimagnetic minerals occurs and the susceptibility signal is negatively correlated with pedogenesis (Liu et al., 2003). This by itself indicates that precipitation was likely to have been very high during this interval.

In summary, a wet climate prevailed across the CLP in the early Pliocene. At the same time, the hematite/goethite ratio from the SCS also indicates enhanced precipitation amount and the smectite/kaolinite ratio indicates increased seasonality at ~4.8 Ma (Fig. 7 i and j), and thus the enhancement of the palaeo-EASM (Clift et al., 2006, 2014). Therefore, we regard the climatic change evident in XSZ section as the result of the expansion of the palaeo-EASM.

The remarkably increased amplitude of the 41-kyr filtered components from the XSZ section and the deep sea  $\delta^{18}\text{O}$  record at about 4.8 Ma indicates the expansion of the palaeo-EASM may have been related to changes in global temperature and ice volume. Furthermore, a decrease in the input of ice-rafted debris to the sediments of the subarctic northwest Pacific was synchronous with the expansion of the palaeo-EASM during the early Pliocene (Fig. 6). In addition, from 4.8-4.7 Ma and 4.6-4.25 Ma, the high values of the three pedogenic indices at the XSZ section indicate that strong pedogenic intensity corresponded with high SSTs in the Eastern Equatorial Pacific (EEP). This coherence between the record of the XSZ section and marine records implies that phases of enhanced precipitation were correlative with changes in SST and ice volume (or temperature) at northern high latitudes.

#### **5.4 Possible driver of palaeo-EASM expansion during early Pliocene**

Ding (2001) proposed that the uplift of the TP to a critical elevation resulted in an enhanced summer monsoon system during 4.8-4.1 Ma. TP uplift was shown to have had

profound effects on the EASM in terms of its initiation and strength as well as changing the distribution of the band of high precipitation in East Asia (Li et al., 1991, 2014; An et al., 2001). A detailed modeling study demonstrated that the uplift of the northern TP mainly resulted in an intensified summer monsoon and increased precipitation in northeast Asia (Zhang et al., 2012). From 8.26-4.96 Ma, massive deltaic conglomerates were widely deposited and the sediment deposition rate increased, indicating the uplift of the Qilian Mountains (Song et al., 2001). At the same time, the Laji Mountains underwent pronounced uplift by thrusting at ~8 Ma, which resulted in the current basin-range pattern (Li et al., 1991; Fang et al., 2005a; Zheng et al., 2000). However, geological and palaeontological records indicate that the uplift of the eastern and northern margins of the TP was very minor from the late Miocene to the middle Pliocene (Li et al., 1991, 2015; Zheng et al., 2000; Fang et al., 2005a, 2005b). Therefore, we speculate that uplift of the TP was not the major cause of the expansion of the palaeo-EASM at ~4.8 Ma.

The occurrence of humid climate across the CLP was synchronous with the gradual closure of the Panama Seaway (Keigwin et al., 1978; O'Dea et al., 2016). Nie (2014) proposed that the freshening of Eastern Equatorial and North Pacific surface water, resulting from the closure of the Panama Seaway since 4.8 Ma (Haug et al., 2001), led to sea ice formation in the North Pacific Ocean, which enhanced the high-pressure cell over the Pacific and increased the strength of southerly and southeasterly winds. However, there was a warming trend in the Northern Hemisphere at 4.6 Ma (Haug et al., 2005; Lawrence et al., 2006). The gradual closure of the Panama Seaway resulted in the reorganization of surface currents in the Atlantic Ocean. Notably, the Gulf Stream was enhanced and began to transport

warm surface waters to high northern latitudes, thus strengthening the Atlantic meridional overturning circulation and warming the Arctic (Haug and Tiedemann, 1998; Haug et al., 2005). Three independent proxies from an early Pliocene peat deposit in the Canadian High Arctic indicate that Arctic temperatures were 19 °C warmer during the early Pliocene than today (Ballantyne et al., 2010). This warmth is also confirmed by other records from high northern latitude regions: diatom abundances and assemblages, pollen data, magnetic susceptibility and sedimentological evidence from Siberia all indicate that the climate was warm and wet in the early Pliocene (Memb B. D. P., 1997, 1999). The warming of the northern high latitude region led to increases in summer temperature in the mid-latitudes of Eurasia. On the other hand, equatorial SSTs remained stable or cooled slightly (Brierley et al., 2009; Fedorov et al., 2013), and thus the land-ocean thermal contrast was intensified. Furthermore, external heating derived from a reduced ice albedo at high northern latitudes also enhanced the thermal contrast between the Pacific and Eurasian regions (Dowsett et al., 2010). This large land-ocean thermal contrast was essential for enhancing the palaeo-EASM. On the other hand, the unusually warm Arctic and small meridional heat gradient in the Northern Hemisphere pushed the Intertropical Convergence Zone northward (Chang et al., 2013; Sun et al., 2015), which weakened the westerly circulation and thus facilitated the northwestward expansion of the palaeo-EASM.

Figure 6 shows that high values of pedogenic indices in the XSZ section correspond with high SSTs in the EEP. This appears to be contradictory to the case of the modern ENSO (when the EEP temperature is high, the precipitation amount in the western CLP is low). The discrepancy may indicate that the nature of sea-air interactions during the early Pliocene was



different from today. From 4.8-4.0 Ma, the thermohaline circulation was reorganizing and creating a precondition for the development of the modern equatorial Pacific cold tongue (Chaisson and Ravelo, 2000). Several crucial changes linked with the summer monsoon occurred: There was a vast expansion of the western Pacific warm pool into subtropical regions in the early Pliocene (Brierley et al., 2009; Fedorov et al., 2013), and temperatures at the edge of the warm pool showed a warming trend of  $\sim 2^{\circ}\text{C}$  from the latest Miocene to the early Pliocene (Karas et al., 2011). This enhanced thermal state of the WEP warm pool significantly enhanced the summer monsoon and its northward extension. Today, when the northern part of the western Pacific warm pool is warm, convection over and around the Philippines is enhanced; and subsequently, the northern extent of the western Pacific subtropical high shifts northwards from the Yangtze River valley to the Yellow River valley and moisture is introduced across the entire CLP (Huang et al., 2003). Further research is needed to determine if this was also the case during the early Pliocene. However, the warming and freshening of the subtropical Pacific would have promoted increased evaporation which would have provided enhanced moisture for the palaeo-EASM, resulting in increased rainfall across the CLP.

In conclusion, we infer that the warming of high northern latitudes, accompanied by the vast poleward expansion of the tropical warm pool into subtropical regions and the freshening of the subtropical Pacific, facilitated the expansion of the palaeo-EASM during the early Pliocene.

## **6. Conclusions**

The continuous late Miocene-Pliocene red clay sequence preserved on the planation

surface in the NE Tibetan Plateau provides the opportunity to elucidate the history of the Asian monsoon in the western CLP. Multi-proxy records from the XSZ section, together with other paleoclimatic records from the CLP, reveal two intervals of major climatic change from 6.7-3.6 Ma. During the first interval (6.7-4.8 Ma), both the amount and variability of precipitation over the XSZ section were small; however, they were much greater in the central and eastern CLP. Thus, the palaeo-EASM had little influence on the climate of the western CLP at this time. During the second interval (4.8-3.6 Ma), the records from the XSZ section indicate that both the amount and variability of precipitation were large. The climate was characterized by abrupt increases in the seasonality of precipitation, which attests to a major northwestward extension and enhancement of the summer monsoon. Obviously, multiple paleoclimatic proxies show that the strongest summer monsoon occurred during 4.60-4.25 Ma. The expansion of the palaeo-EASM may have been caused by warming of the Arctic region, a vast poleward expansion of the tropical warm pool into subtropical regions, and freshening of the subtropical Pacific in response to the closure of the Panamanian Seaway during the early Pliocene.

## **Acknowledgements**

We thank Ai Song, Jia Liu, Shanpin Liu and Jun Zhang for the drilling operation and Fengxia Yu for her early experimental work. We thank Jan Bloemendal for modifying and polishing the language. We specially thank Ran Feng and three anonymous reviewers for their suggestions and comments that helped improve the paper. This work was supported by the National Natural Science Foundation of China (grants 41330745 and 41401214) and the

Key Laboratory of Continental Collision and Plateau Uplift, Institute of Tibetan Plateau  
Research (LCP201602).

## References

An, Z. S., Kutzbach, J. E., Prell, W. L., Porter, S. C.: Evolution of Asian monsoons and phased uplift of the  
Himalayan Tibetan plateau since Late Miocene times. *Nature*, 411, 62–66, 2001.

An, Z. S.: Late Cenozoic Climate Change in Asia. Springer Netherlands, 2014.

Ao, H., Roberts, A. P., Dekkers, M. J., Liu, X., Rohling, E. J., Shi, Z., An, Z. S., and Zhao, X.: Late  
Miocene–Pliocene Asian monsoon intensification linked to Antarctic ice-sheet growth. *Earth &  
Planetary Science Letters*, 444, 75–87, 2016. Avery, B. W., and Bascomb, C. L.: Soil survey laboratory  
methods /, 1974.

Ballantyne, A. P., Greenwood, D. R., Sinningh-Damste, J. S., Csank, A. Z., Eberle, J. J., and Rybczynski,  
N.: Significantly warmer arctic surface temperatures during the Pliocene indicated by multiple  
independent proxies. *Geology*, 38(7), 603–606, 2010.

Brierley, C. M., Fedorov, A. V., Liu, Z., Herbert, T. D., Lawrence, K. T., and Lariviere, J. P.: Greatly  
expanded tropical warm pool and weakened Hadley circulation in the early Pliocene. *Science*,  
323(5922), 1714–8, 2009.

Brierley, C. M., and Fedorov, A. V.: Relative importance of meridional and zonal sea surface temperature  
gradients for the onset of the ice ages and Pliocene–Pleistocene climate evolution. *Paleoceanography*,  
25(4), 2010.

Buggle, B., Glaser, B., Hambach, U., Gerasimenko, N., and Markovi, S.: An evaluation of geochemical  
weathering indices in loess–paleosol studies. *Quaternary International*, 240(1–2):12–21, 2011.

593 Chaisson, W. P., and Ravelo, A. C.: Pliocene development of the east-west hydrographic gradient in the  
594 equatorial Pacific. *Paleoceanography*, 15(5), 497-505, 2000.

595 Chang, H., An, Z. S., Wu, F. L., Jin, Z., Liu, W. G., and Song, Y. G.: A Rb/sr record of the weathering  
596 response to environmental changes in westerly winds across the tarim basin in the late Miocene to the  
597 early Pleistocene. *Palaeogeography Palaeoclimatology Palaeoecology*, 386(6), 364-373, 2013.

598 Clift, P. D.: Controls on the erosion of cenozoic asia and the flux of clastic sediment to the ocean. *Earth &*  
599 *Planetary Science Letters*, 241(3-4), 571-580, 2006.

600 Clift, P. D., Hodges, K. V., Heslop, D., Hannigan, R., Long, H. V., and Calves, G.: Correlation of  
601 Himalayan exhumation rates and Asian monsoon intensity. *Nature Geoscience*, 1(12),  
602 doi:10.1038/ngeo351, 2008.

603 Clift, P. D., Wan, S. M., and Blusztajn, J.: Reconstructing chemical weathering, physical erosion and  
604 monsoon intensity since 25 ma in the northern south china sea: a review of competing proxies. *Earth-*  
605 *Science Reviews*, 130(3), 86-102, 2014.

606 Compo, G., Whitaker, J., Sardeshmukh, P., and Mccoll, C.: The quality control system of the 20th century  
607 reanalysis dataset. *Egu General Assembly*, 15, 2013.

608 Ding, Z. L., Yang, S. L., Sun, J. M., and Liu, T. S.: Iron geochemistry of loess and red clay deposits in the  
609 chinese loess plateau and implications for long-term asian monsoon evolution in the last 7.0 ma. *Earth*  
610 *& Planetary Science Letters*, 185(1), 99-109, 2001.

611 Dowsett, H. J., Robinson, M., Haywood, A., Salzmann, U., Hill, D., Sohl, L. E., Chandler, M., Williams,  
612 M., Foley, K., and Stoll, D. K.: The PRISM3D paleoenvironmental reconstruction. *Stratigraphy*, 7,  
613 123-139, 2010.

614 Fedorov, A. V., Brierley, C. M., Lawrence, K. T., Liu, Z., Dekens, P. S., and Ravelo, A. C.: Patterns and

615 mechanisms of early Pliocene warmth. *Nature*, 496 (7443), 43, 2013.

616 Fang, X. M, Li, J. J, Derbyshire, E., Fitzpatrick, E. A., and Kemp, R. A.: Micromorphology of the Beiyuan  
617 loess-paleosol sequence in Gansu province, China: geomorphological and paleoenvironmental  
618 significance. *Palaeogeography Palaeoclimatology Palaeoecology*, 111(3–4), 289-303, 1994.

619 Fang, X. M., Ono, Y., Fukusawa, H., Pan, B. T., Li, J. J., Guan, D. H., Oi. K., Tsukamoto, S., Torii, M.,  
620 and Mishima, T.: Asian summer monsoon instability during the past 60,000 years: magnetic  
621 susceptibility and pedogenic evidence from the western Chinese Lloess plateau. *Earth & Planetary  
622 Science Letters*, 168(3–4), 219-232, 1999.

623 Fang, X. M., Yan, M. D., Voo, R. V. D., Rea, D. K., Song, C. H., Parés, J. M., Gao J. P., Nie J. S., and Dai  
624 S.: Late Cenozoic deformation and uplift of the NE Tibetan plateau: evidence from high-resolution  
625 magnetostratigraphy of the Guide basin, Qinghai province, China. *Geological Society of America  
626 Bulletin*, 117(9), 1208-1225, 2005a.

627 Fang, X., Zhao, Z. J., Li J. J., Yan, M. D, Pan, B. T., Song, C. H., and Dai, S.: Magnetostratigraphy of the  
628 late Cenozoic Laojunmiao anticline in the northern Qilian mountains and its implications for the  
629 Northern Tibetan plateau uplift. *Science in China*, 48(7), 1040-1051, 2005b.

630 Fang, X. M, Wu, F. L., Hai, W. X., Wang, Y. D., Zhang, X. Z., and Zhang, W. L.: Plio-Pleistocene drying  
631 process of Asian inland-sporopollen and salinity records from Yahu section in the central Qaidam  
632 basin( in Chinese ). *Quaternary Sciences* 28(5): 874-882, 2008.

633 Fedo, C. M., Nesbitt, H. W., and Young, G. M.: Unraveling the effects of potassium metasomatism in  
634 sedimentary rocks and paleosols, with implications for paleoweathering conditions and  
635 provenance. *Geology*, 23(10), 921-924, 1995.

636 Guo, Z. T., Peng, S. Z., Hao, Q. Z., Biscaye, P. E., and Liu, T. S.: Origin of the Miocene–Pliocene red-

637 earth formation at Xifeng in northern China and implications for paleoenvironments.

638 Palaeogeography Palaeoclimatology Palaeoecology, 170(1-2), 11-26, 2001.

639 Han, W., Fang, X., Berger, A., and Yin, Q.: An astronomically tuned 8.1 ma eolian record from the

640 Chinese Loess plateau and its implication on the evolution of Asian monsoon. Journal of Geophysical

641 Research Atmospheres, 116(D24114), 2011.

642 Haug, G. H., and Tiedemann, R.: Effect of the formation of the isthmus of Panama on Atlantic ocean

643 thermohaline circulation. Nature, 393(3), 673-676, 1998.

644 Haug, G. H., Tiedemann, R., Zahn, R., and Ravelo, A. C.: Role of Panama uplift on oceanic freshwater

645 balance. Geology, 29(3), 207-210, 2001.

646 Haug, G. H., Ganopolski, A., Sigman, D. M., Rosell-Mele, A., Swann, G. E., Tiedemann, R., Jaccard, S. L.,

647 Bollmann, B. J., Maslin, M. A., Leng, M. J., and Eglinton, G.: North pacific seasonality and the

648 glaciation of north America 2.7 million years ago. Nature, 433(7028), 821-825, 2005.

649 Herbert, T. D., Peterson, and Liu, Z.: Tropical ocean temperatures over the past 3.5 million

650 years. Science, 328(5985), 1530-4, 2010.

651 Herbert, T. D., Lawrence, K. T., Tzanova, A., Peterson, L. C., Caballero-gill, R., and Kelly, C. S.: Late

652 Miocene global cooling and the rise of modern ecosystems. Nature Geoscience, 9(11), 2016.

653 Huang, R. H., Zhou L.T., and Chen, W.: The progresses of recent studies on the variabilities of the East

654 Asian monsoon and their causes, Adv. Atmos. Sci., 20, 55-69, 2003.

655 Jansen, E., and Sjøholm, J.: Reconstruction of glaciation over the past 6 Myr from ice-borne deposits in the

656 Norwegian sea. Nature, 349(6310), 600-603, 1991.

657 Karas, C., Nürnberg, D., Tiedemann, R., and Garbe-Schönberg, D. : Pliocene climate change of the

658 southwest Pacific and the impact of ocean gateways. Earth & Planetary Science Letters, 301(1–2),

659 117-124, 2011.

660 Keigwin, L. D.: Pliocene closing of the isthmus of Panama, based on biostratigraphic evidence from  
661 nearby Pacific ocean and Caribbean sea cores. *Geology*, 6(10), 630, 1978. King, T.: Quantifying non-  
662 linearity and geometry in time series of climate. *Quaternary Science Reviews* 15, 247-266, 1996.

663 Laskar, J.: Long-term solution for the insolation quantities of the earth. *Proceedings of the International  
664 Astronomical Union*, 2(14), 101-106, 2004.

665 Lawrence, K. T., Liu, Z., and Herbert, T. D.: Evolution of the eastern tropical pacific through Plio-  
666 Pleistocene glaciation. *Science*, 312(5770), 79-83, 2006.

667 Liang, L., Sun, Y., Beets, C. J., Prins, M. A., Wu, F., and Vandenberghe, J.: Impacts of grain size sorting  
668 and chemical weathering on the geochemistry of Jingyuan loess in the northwestern Chinese Loess  
669 plateau. *Journal of Asian Earth Sciences*, 69(12), 177-184, 2013.

670 Li, F. J., Rousseau, D. D., Wu, N., Hao, Q., and Pei, Y.: Late Neogene evolution of the East Asian  
671 monsoon revealed by terrestrial mollusk record in western Chinese Loess plateau: from winter to  
672 summer dominated sub-regime. *Earth & Planetary Science Letters*, 274(3–4), 439-447, 2008.

673 Li, J.J.: The environmental effects of the uplift of the Qinghai-Xizang plateau. *Quaternary Science  
674 Reviews*, 10(6), 479-483, 1991.

675 Li, J.J., Fang, X., Song, C., Pan, B., Ma, Y., and Yan, M., Late Miocene–quaternary rapid stepwise uplift  
676 of the ne Tibetan plateau and its effects on climatic and environmental changes. *Quaternary Research*,  
677 81(3), 400-423, 2014.

678 Li, J. J., Zhou, S. Z., Zhao, Z. J., and Zhang, J.: The Qingzang movement: the major uplift of the Qinghai-  
679 Tibetan plateau. *Science China Earth Sciences*, 58(11), 2113-2122, 2015.

680 Li, J. J., Ma, Z. H., Li, X. M., Peng, T. J., Guo, B. H., Zhang, J., Song, C. H., Liu, J. Hui, Z. C., Yu, H.,

681 Ye, X. Y., Liu, S. P., Wang, X. X.: Late Miocene-Pliocene geomorphological evolution of the  
 682 Xiaoshuizi peneplain in the Maxian Mountains and its tectonic significance for the northeastern  
 683 Tibetan Plateau. *Geomorphology*. 295 393-405, 2017.

684 Liu, X. M., Rolph, T., An, Z., and Hesse, P.: Paleoclimatic significance of magnetic properties on the red  
 685 clay underlying the loess and paleosols in China. *Palaeogeography Palaeoclimatology Palaeoecology*,  
 686 199(1), 153-166, 2003.

687 Liu, C. Q., Masuda, A., Okada, A., Yabuki, S., Zhang, J., and Fan, Z. L.: A geochemical study of loess and  
 688 desert sand in northern China: implications for continental crust weathering and composition.  
 689 *Chemical Geology*, 106 (3-4), 359-374, 1993.

690 Liu, Q., Jackson, M. J., Yu, Y., Chen, F., Deng, C., and Zhu, R.: Grain size distribution of pedogenic  
 691 magnetic particles in Chinese loess/paleosols. *Geophysical Research Letters*, 312(22), 359-393, 2004.

692 Liu, Q., Torrent, J., Maher, B. A., Yu, Y., Deng, C. L., Zhu, R., and Zhao X. X.: Quantifying grain size  
 693 distribution of pedogenic magnetic particles in Chinese loess and its significance for pedogenesis.  
 694 *Journal of Geophysical Research Atmosphere*, 110(B11), 2005.

695 Liu, W., Liu, Z., An, Z., Sun, J., Chang, H., Wang, N., and Dong, J. B.: Late Miocene episodic lakes in the  
 696 arid Tarim basin, western China. *Proceedings of the National Academy of Sciences*, 111(46), 16292-6,  
 697 2014.

698 Lu, H., Zhang, F., Liu, X., and Duce, R. A: Periodicities of palaeoclimatic variations recorded by loess-  
 699 paleosol sequences in China. *Quaternary Science Reviews*, 23(18–19), 1891–1900, 2004.

700 Ma, Y. Z., Wu, F. L., Fang, X. M., Li, J. J., An, Z. S., and Wei, W.: Pollen record from red clay sequence  
 701 in the central Loess plateau between 8.10 and 2.60 Ma. *Chinese Science Bulletin*, 50(19), 2234-2243,  
 702 2005.



703 Memb, B. D. P.: Preliminary results of the first scientific drilling on lake Baikal, Buguldeika site,  
704 southeastern Siberia. *Quaternary International*, 37(2), 3-17, 1997.

705 Memb, B. D. P.: Continuous paleoclimate record recovered for last 5 million years. *Eos Transactions*  
706 *American Geophysical Union*, 78(51), 597-601, 1999. Mudie, P. J., and Helgason, J.: Palynological  
707 evidence for Miocene climatic cooling in eastern iceland about 9.8 myr ago. *Nature*, 303(5919), 689-  
708 692, 1983.

709 Nesbitt, H. W., Markovics, G., and Price, R. C.: Chemical processes affecting alkalis and alkaline earths  
710 during continental weathering. *Geochimica Et Cosmochimica Acta*, 44(11), 1659-1666, 1980.

711 Nie, J. S., Stevens, T., Song, Y., King, J. W., Zhang, R., Ji, S. C, Gong L. S., and Cares, D.: Pacific  
712 freshening drives Pliocene cooling and Asian monsoon intensification. *Scientific Reports*, 4, 5474,  
713 2014.

714 O'Dea, A., Lessios H. A., Coates, A. G., Eytan, R. I., Restrepo-Moreno, S. A., Cione, A. L., Collins, L. S.,  
715 Queiroz, A. D., Farris, D. W., Norris, R. D., Stallard, R. F., Woodburne, M. O., Aguilera, O., Aubry,  
716 M. P., Berggren, W. A., Budd, A. F., Cozzuol, M. A., Coppard, S. E., Duque-Caro, H., Finnegan, S.,  
717 Gasparini, G. M., Grossman, E. L., Johnson, K. G., Keigwin, L. D., Knowlton, N., Leigh, E. G.,  
718 Leonard-Pingel, J. S., Marko, P. B., Pyenson, N. D., Rachello-Dolmen, P. G., Soibelzon, E.,  
719 Soibelzon, L., Todd, J. A., Vermeij, G. J., and Jackson, J. B. C.: Formation of the Isthmus of Panama.  
720 *Science Advances*, 2(8), 2016.

721 Pagani, M., Liu, Z., Lariviere, J., and Ravelo, A. C.: High earth-system climate sensitivity determined from  
722 Pliocene carbon dioxide concentrations. *Nature Geoscience*, 3(1), 27-30, 2010.

723 Rossinsky V. J., and Swart, P. K.: Influence of climate on the formation and isotopic composition of  
724 calcretes. In: Swart, P.K., Lohmann, K.C., McKenzie, J., Savin, S. (Eds.), *Climate Change in*  
725 *Continental Isotopic Records*, American Geophysical Union: Geophysical Monography, 78, pp. 67-75,

1993.

Song, C. H., Fang, X. M., Li, J. J., Gao, J., Zhao, Z. J., and Fan, M. J.: Tectonic uplift and sedimentary evolution of the Jiuxi basin in the northern margin of the Tibetan plateau since 13 Ma BP. *Science China Earth Sciences*, 44(1), 192-202, 2001.

Song, Y. G., Fang, X. M., Torii, M., Ishikawa, N., Li, J. J., and An, Z. S.: Late Neogene rock magnetic record of climatic variation from Chinese eolian sediments related to uplift of the Tibetan plateau. *Journal of Asian Earth Sciences*, 30(2), 324-332, 2007.

Sun, D. H., Bloemendal, J., Rea, D. K., An, Z. S., Vandenberghe, J., and Lu, H., Su, R. X., and Liu, T. : Bimodal grain-size distribution of Chinese loess, and its palaeoclimatic implications. *Catena*, 55(3), 325-340, 2004.

Sun, J. M., and Liu, T. S. : The age of the Taklimakan desert. *Science*, 312 (5780), 1612-1621, 2006a.

Sun, J. M., and Huang, X.: Half-precessional cycles recorded in Chinese loess: response to low-latitude insolation forcing during the last interglaciation. *Quaternary Science Reviews*, 25(9–10), 1065-1072, 2006b.

Sun, J. M., Liu, W. G., Liu, Z., Deng, T., Windley, B. F., and Fu, B.: Extreme aridification since the beginning of the Pliocene in the Tarim basin, western China. *Palaeogeography Palaeoclimatology Palaeoecology*, 2017.

Sun, Y. B., Lu, H. Y., and An, Z. S.: Grain size of loess, palaeosol and red clay deposits on the Chinese Loess plateau: significance for understanding pedogenic alteration and palaeomonsoon evolution. *Palaeogeography Palaeoclimatology Palaeoecology*, 241(1), 129-138, 2006c.

Sun, Y. B., An, Z. S., Clemens, S. C., Bloemendal, J., and Vandenberghe, J.: Seven million years of wind and precipitation variability on the Chinese Loess plateau. *Earth & Planetary Science Letters*, 297(3–

748 4), 525-535, 2010.

749 Sun, Y. B., Kutzbach, J., An, Z., Clemens, S., Liu, Z., Liu, W., Liu, X. D., Shi, Z. G., Zheng, W. P., Liang,  
750 L., Yan, Y., and Li, Y.: Astronomical and glacial forcing of East Asian summer monsoon  
751 variability. *Quaternary Science Reviews*, 115, 132-142, 2015.

752 Tripathi, A. K., Roberts, C. D., and Eagle, R. A.: Coupling of CO<sub>2</sub> and ice sheet stability over major climate  
753 transitions of the last 20 million years. *Science*, 326(5958), 1394-1397, 2009.

754 Tang, H., Micheels, A., Eronen, J., and Fortelius, M.: Regional climate model experiments to investigate  
755 the Asian monsoon in the late Miocene. *Climate of the Past*, 7(3), 847-868, 2011.

756 Vandenberghe, J., H. Lu, D. Sun, J. Huissteden, V., and Konert, M.: The late Miocene and Pliocene  
757 climate in East Asia as recorded by grain size and magnetic susceptibility of the Red Clay deposits  
758 (Chinese Loess Plateau), *Palaeogeography Palaeoclimatology Palaeoecology*, 204, 239–255,  
759 doi:10.1016/S0031-0182(03)00729-6, 2004.

760 Wan, S. M., Tian, J., Steinke, S., Li, A., and Li, T.: Evolution and variability of the East Asian summer  
761 monsoon during the Pliocene: evidence from clay mineral records of the South China  
762 Sea. *Palaeogeography Palaeoclimatology Palaeoecology*, 293(1–2), 237-247, 2010.

763 Wang, H. B., Chen, F. H., and Zhang, J. W.: Environmental significance of grain size of loess-paleosol  
764 sequence in western part of Chinese Loess plateau. *Journal of Desert Research*, 22(1), 21-26, 2002.

765 Wang, L., Lu, H. Y., Wu, N. Q., Li, J., Pei, Y. P., Tong, G. B., and Peng, S. Z.: Palynological evidence for  
766 Late Miocene-Pliocene vegetation evolution recorded in the red clay sequence of the central Chinese  
767 Loess Plateau and implication for palaeo-environmental change. *Palaeogeography Palaeoclimatology*  
768 *Palaeoecology*. 241, 118–128, 2006.

769 Wara, M. W., Ravelo, A. C., and Delaney, M. L.: Permanent EI ni ño-like conditions during the Pliocene

770 warm period. *Science*, 309(5735), 758-61, 2005.

771 Watanabe, T., Suzuki, A., Minobe, S., Kawashima, T., Kameo, K., & Minoshima, K., Aguilar, Y. M., Wan,  
772 R., Kawahata, H., Sowa, K., Nagai, T., and Kase, T.: Permanent El Niño during the Pliocene warm  
773 period not supported by coral evidence. *Nature*, 471 (7337), 209-211, 2011.

774 Wu, N., Pei, Y., Lu, H., Guo, Z., Li, F., and Liu, T.: Marked ecological shifts during 6.2–2.4 ma revealed  
775 by a terrestrial molluscan record from the Chinese red clay formation and implication for  
776 palaeoclimatic evolution. *Palaeogeography Palaeoclimatology Palaeoecology*, 233(3-4), 287-299,  
777 2006.

778 Xia, D. S., Jia, J., Li, G., Zhao, S., Wei, H. T., and Chen, F. H.: Out-of-phase evolution between summer  
779 and winter East Asian monsoons during the Holocene as recorded by Chinese Loess deposits.  
780 *Quaternary Research*, 81(3), 500-507, 2014.

781 Yang, S. L., Ding, F., and Ding, Z. L.: Pleistocene chemical weathering history of Asian arid and semi-arid  
782 regions recorded in loess deposits of China and Tajikistan. *Geochimica Et Cosmochimica Acta*, 70(7),  
783 1695-1709, 2006.

784 Zachos, J., Pagani, M., Sloan, L., Thomas, E., and Billups, K.: Trends, rhythms, and aberrations in global  
785 climate 65 Ma to present. *Science*, 292(5517), 686-93, 2001.

786 Zhang, R., Jiang, D. B., Liu, X. D., and Tian, Z. P.: Modeling the climate effects of different subregional  
787 uplifts within the Himalaya-Tibetan plateau on Asian summer monsoon evolution. *Science*  
788 *Bulletin*, 57(35), 4617-4626, 2012.

789 Zhang, Y. G., Pagani, M., and Liu, Z.: A 12-million-year temperature history of the tropical Pacific  
790 ocean. *Science*, 344(6179), 84, 2014.

791 Zhao, J. B.: A study of the CaCO<sub>3</sub> illuvial horizons of paleosols and permeated pattern far rain water, J

- 792 Geogr Sci, 15(4), 344-350, 1995.
- 793 Zhao, J. B.: Illuvial CaCO<sub>3</sub> layers of paleosol in loess and its environmental significance, Journal of Xi'an
- 794 Engineering University, 20(3), 46-49, 1998.
- 795 Zheng, H. B, Mcaulay Powell, C., An, Z. S., Zhou, J., and Dong, G. R.: Pliocene uplift of the northern
- 796 Tibetan plateau. Geology, 28(8), 715, 2000.

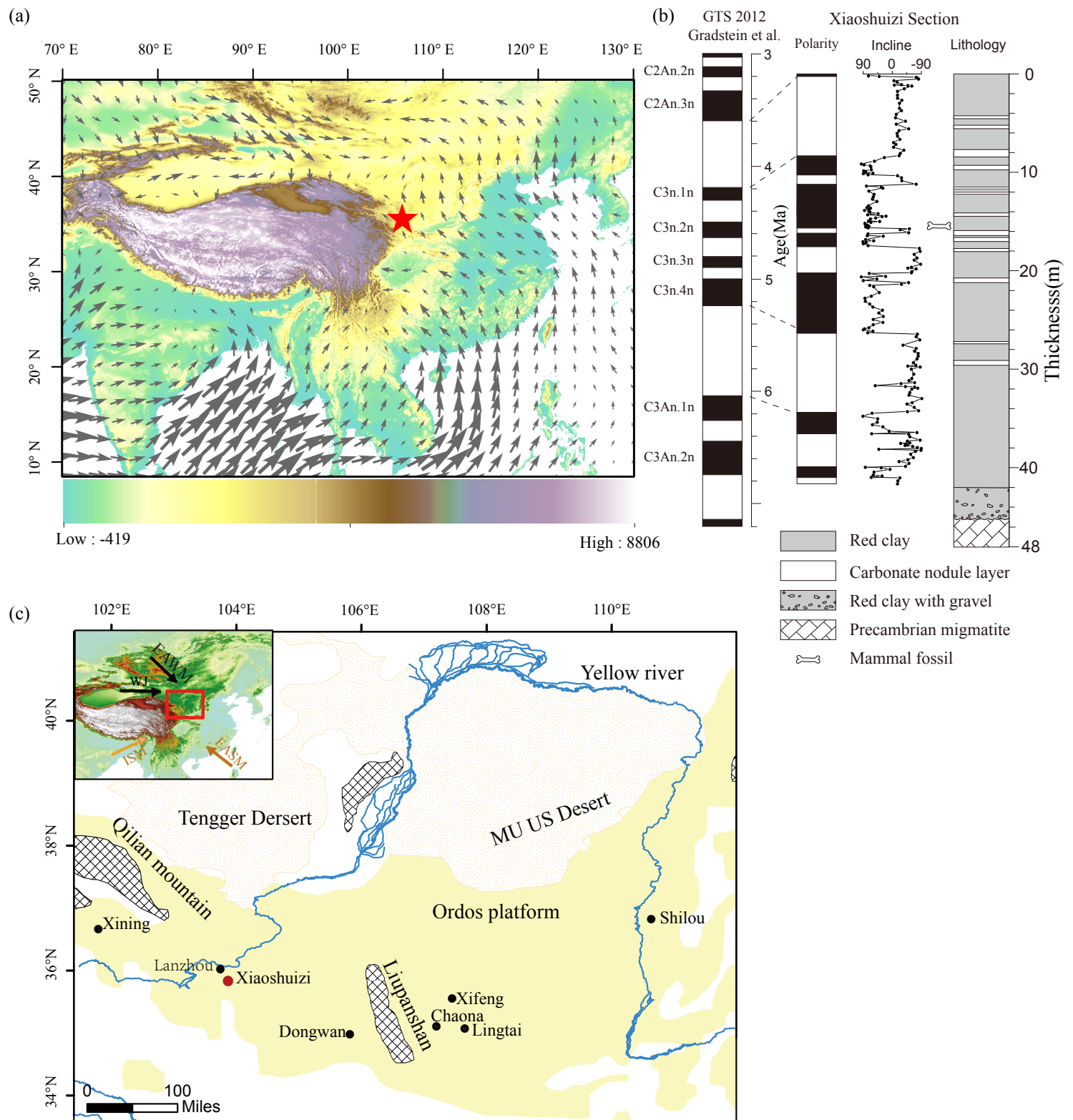


Fig. 1. The location of the study area and atmospheric circulation patterns. (a) 850 mb vector wind averaged from June to August for 1982-2012 based on NOAA Earth System Research Laboratory reanalysis data (Compo et al., 2013). (b) Lithology and magnetostratigraphy of the XSZ drill core. (c) The Chinese Loess Plateau with locations of the studied Xiaoshuizi site and other sections mentioned in the text.

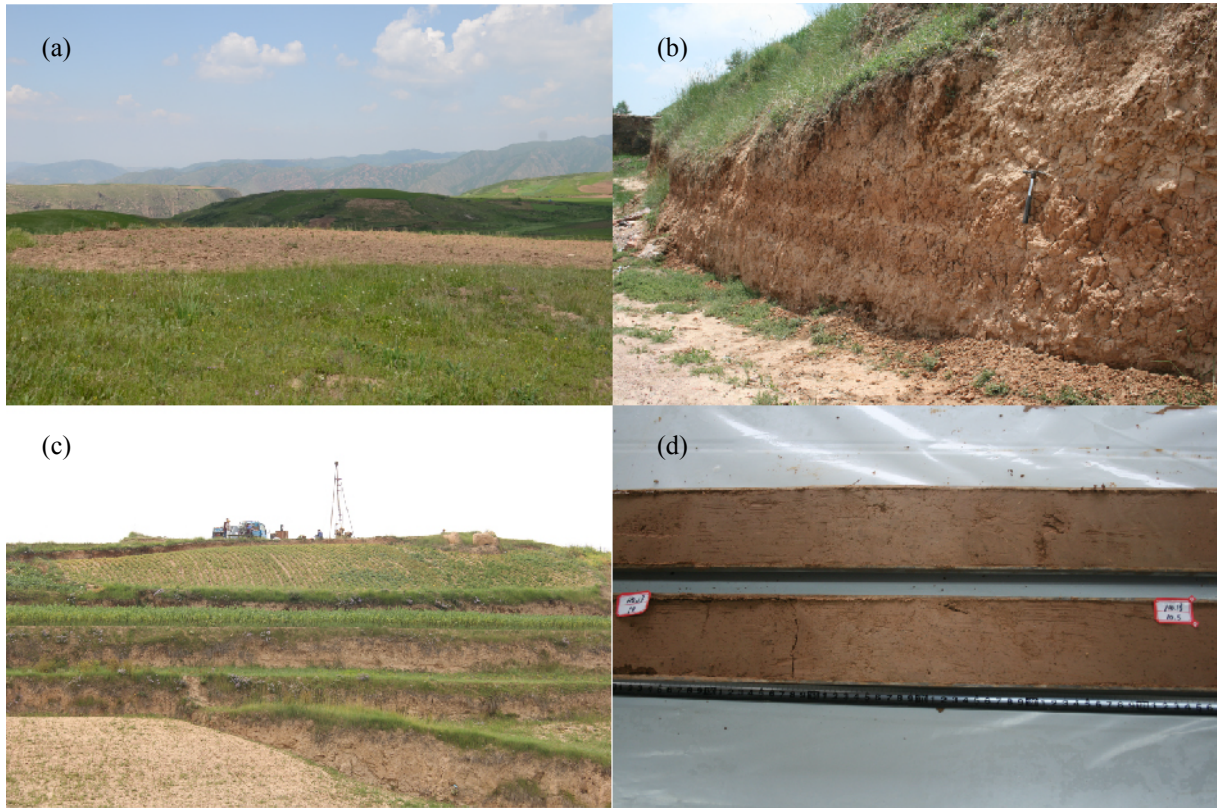


Fig. 2. Photos of the XSZ planation surface and the red clay. (a) XSZ planation surface.

(b) Red clay outcrop, XSZ. (c) Position of the XSZ drilling hole. (d) The XSZ drill core.

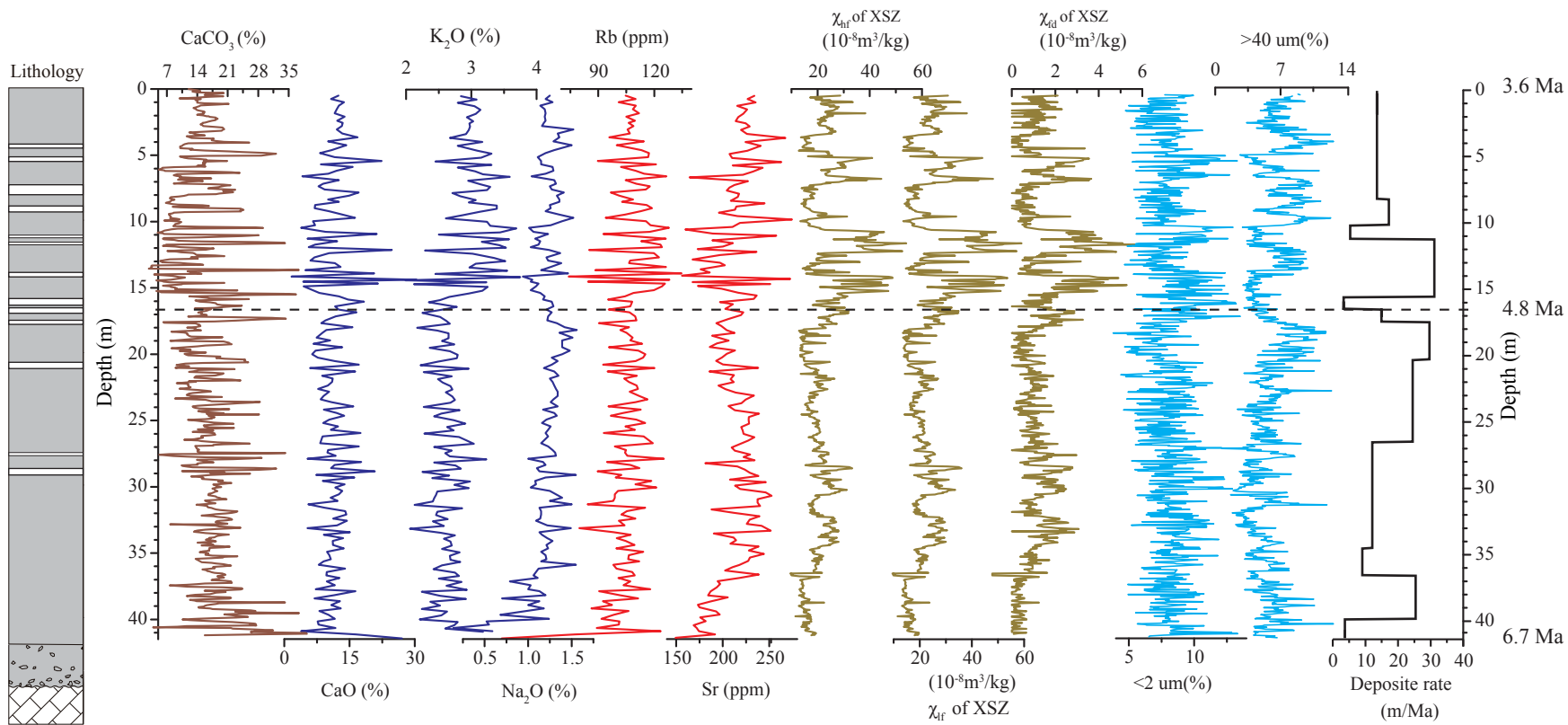


Fig. 3. Variations in carbonate content, major element concentration, minor element concentration, magnetic susceptibility and grain size from the XSZ red clay section, spanning 6.7-3.6 Ma



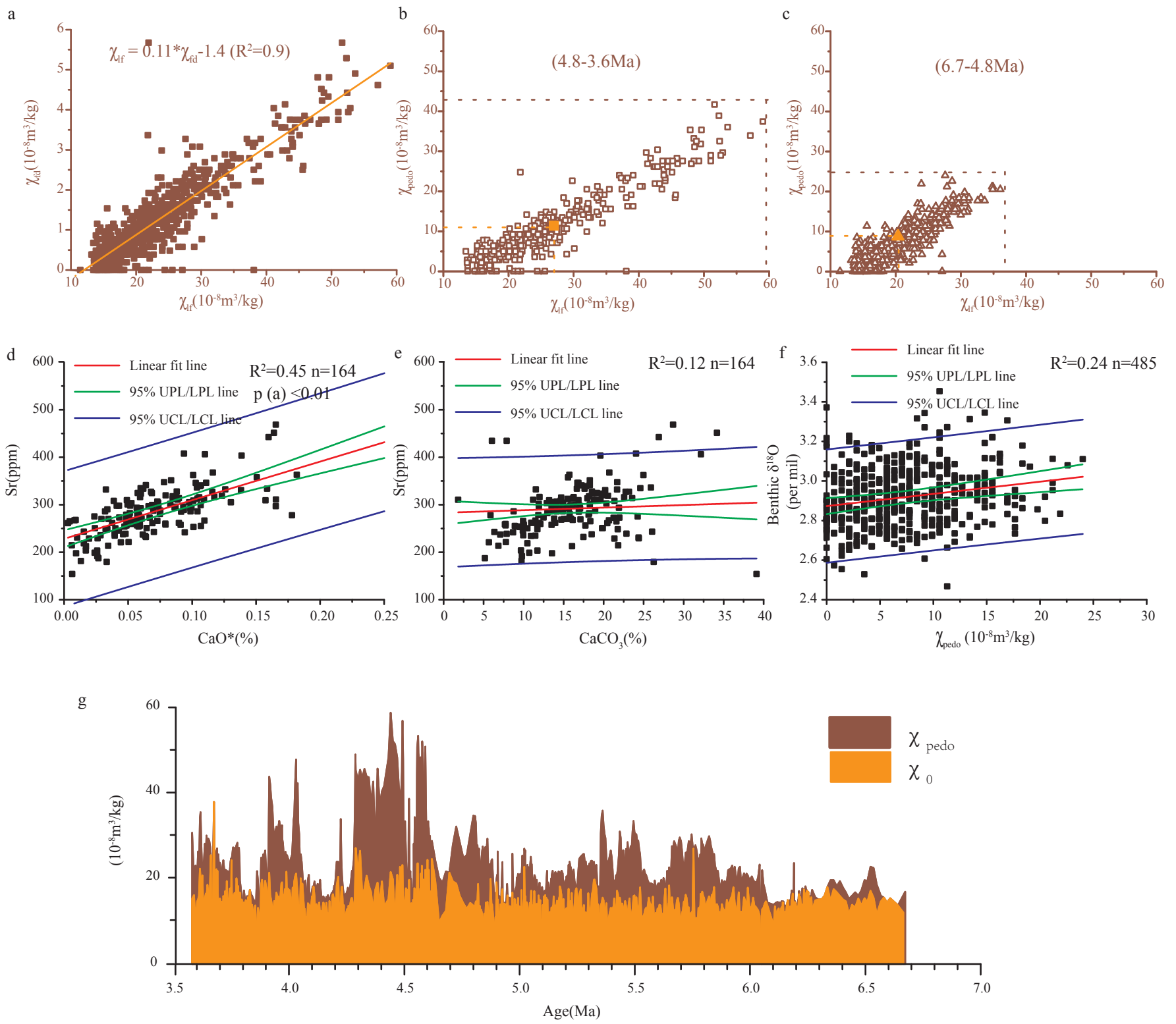


Fig. 4. (a) Scatter plot of  $\chi_{if}$  versus  $\chi_{id}$ . (b) Scatter plot of  $\chi_{if}$  versus  $\chi_{pedo}$  during 4.8-3.6 Ma. (c) Scatter plot of  $\chi_{if}$  versus  $\chi_{pedo}$  during 6.7-4.8 Ma. (d) Scatter plot of Sr versus  $\text{CaCO}_3$ . (e) Scatter plot of Sr versus  $\text{CaO}^*$ . (f) Scatter plot of benthic  $\delta^{18}\text{O}$  versus  $\chi_{pedo}$  during 6.7-4.8 Ma. (g) Separation of  $\chi_{pedo}$  and  $\chi_0$ . Solid squares and triangles are the average values during 4.8-3.6 Ma and 6.7-4.8 Ma, respectively.  $\chi_{pedo}$  is the magnetic susceptibility of pedogenic origin and  $\chi_0$  is the magnetic susceptibility of the detrital material.

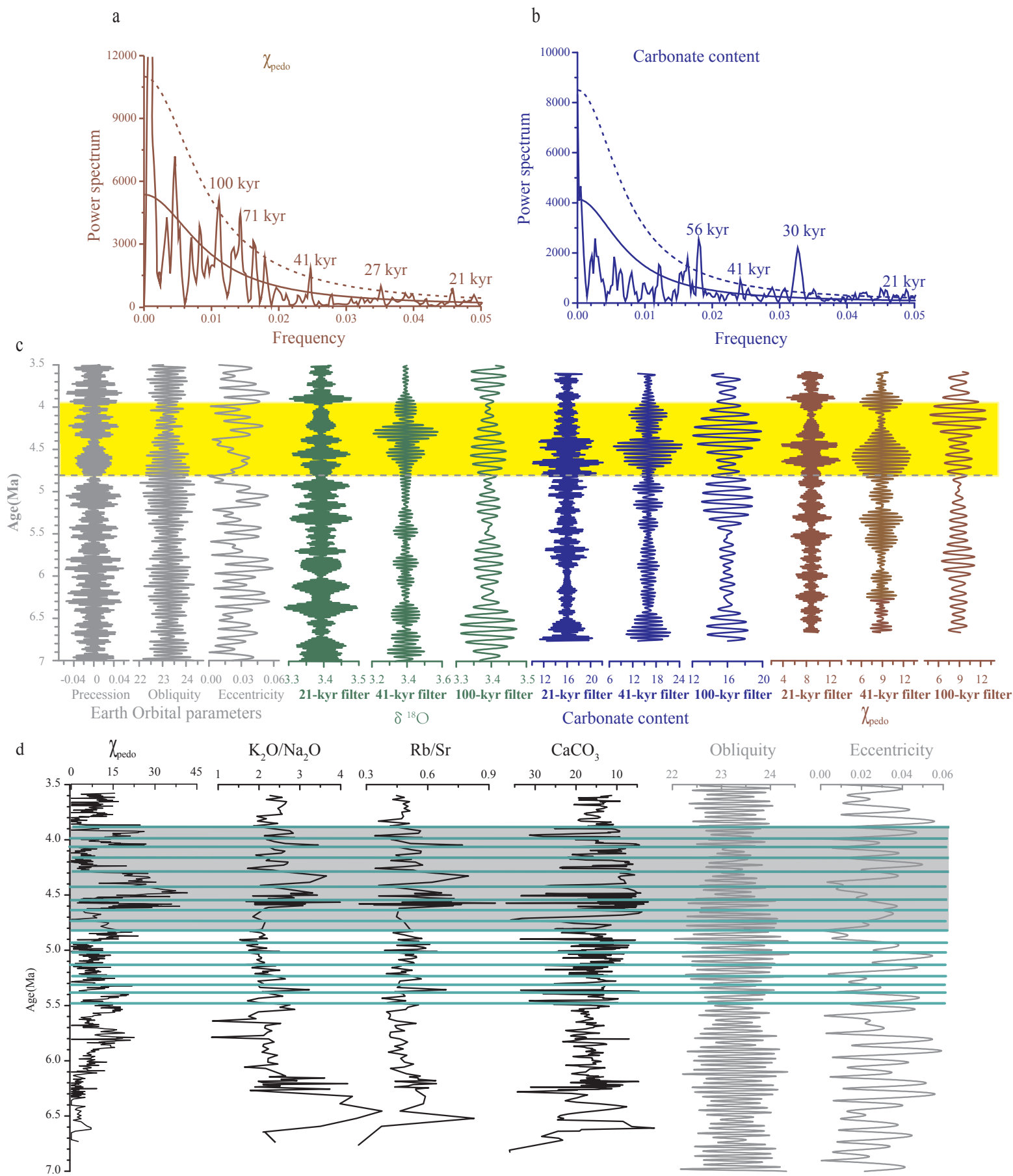


Fig. 5. Spectrum analysis of the red clay. (a)  $\chi_{\text{pedo}}$  and (b) carbonate content (blue). (c) Comparison of orbital parameters (i.e., eccentricity, obliquity and precession, Laskar et al., 2004) with filtered components of the carbonate content,  $\chi_{\text{pedo}}$  and  $\delta^{18}\text{O}$  records (Zachos et al., 2001) at the 18–24 kyr, 36–46 kyr, and 90–110 kyr bands. Yellow shading denotes the largest amplitude of filtered components of carbonate and  $\chi_{\text{pedo}}$  at the three orbital bands. Dashed lines indicate a large shift in the East Asian monsoon circulation occurred around 4.8 Ma. (d) Carbonate, weathering and pedogenesis intensity fluctuations linked to eccentricity and obliquity orbital variations at 4.8–3.9 Ma.

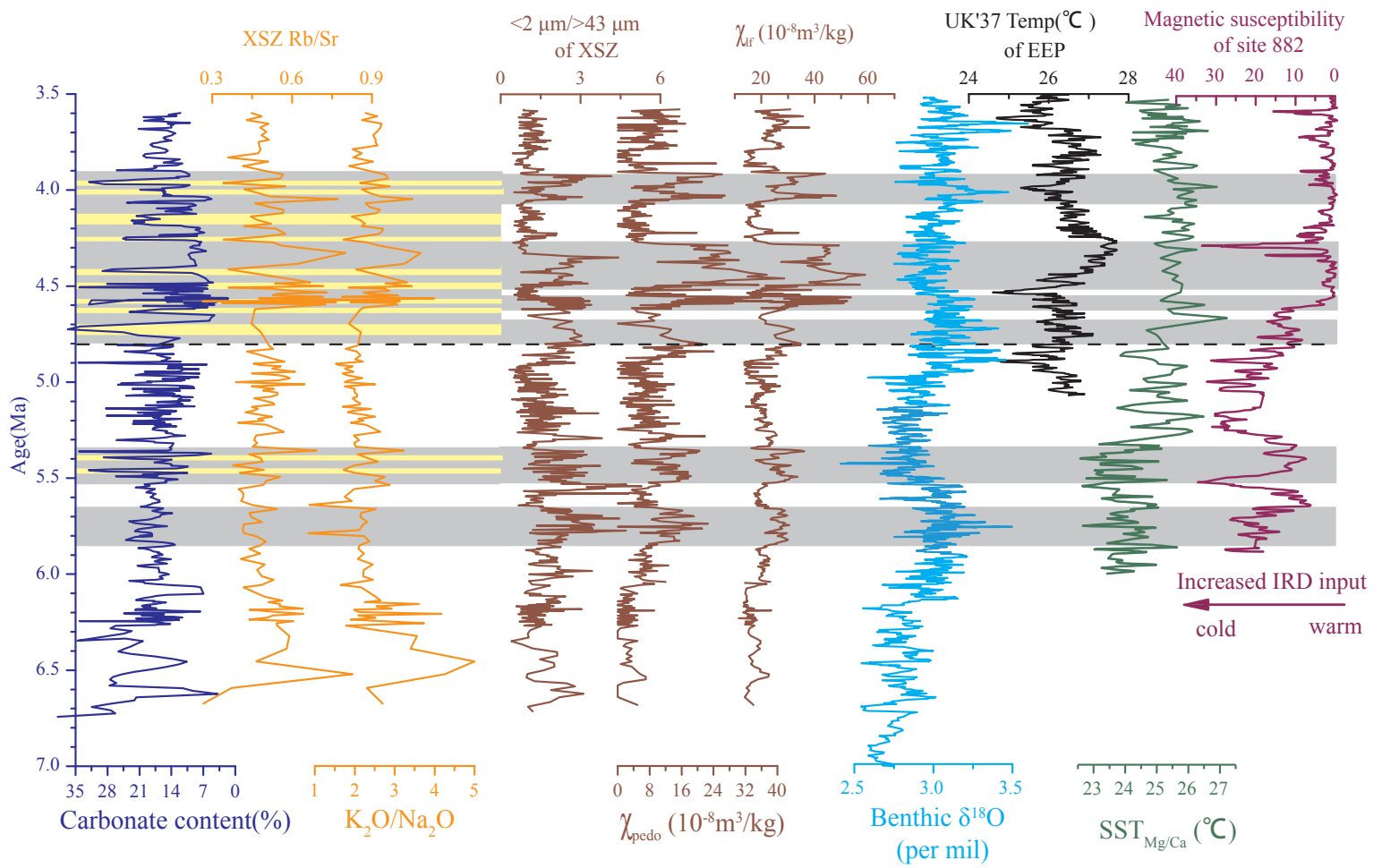


Fig. 6. Temporal evolution of the palaeo-ASM. The dark blue line represents changes in effective precipitation at XSZ, the orange line represents changes in chemical weathering intensity, and the brown lines represent changes in pedogenic intensity. The blue line is the stacked deep-sea benthic foraminiferal oxygen isotope curve compiled from data from DSDP and ODP sites (Zachos et al., 2001). The black line is a reconstruction of sea surface temperature in the eastern equatorial Pacific (EEP) from ODP Site 846 (Lawrence et al., 2006). Green line is a reconstruction temperature at the edge of warm pool from southwest Pacific Ocean Site 590B (Karas et al., 2011). Purple line is magnetic susceptibility from ODP Site 882 (Haug et al., 2005). Gray shading shows relatively wet periods and the light-yellow shading shows intervals of carbonate accumulation.

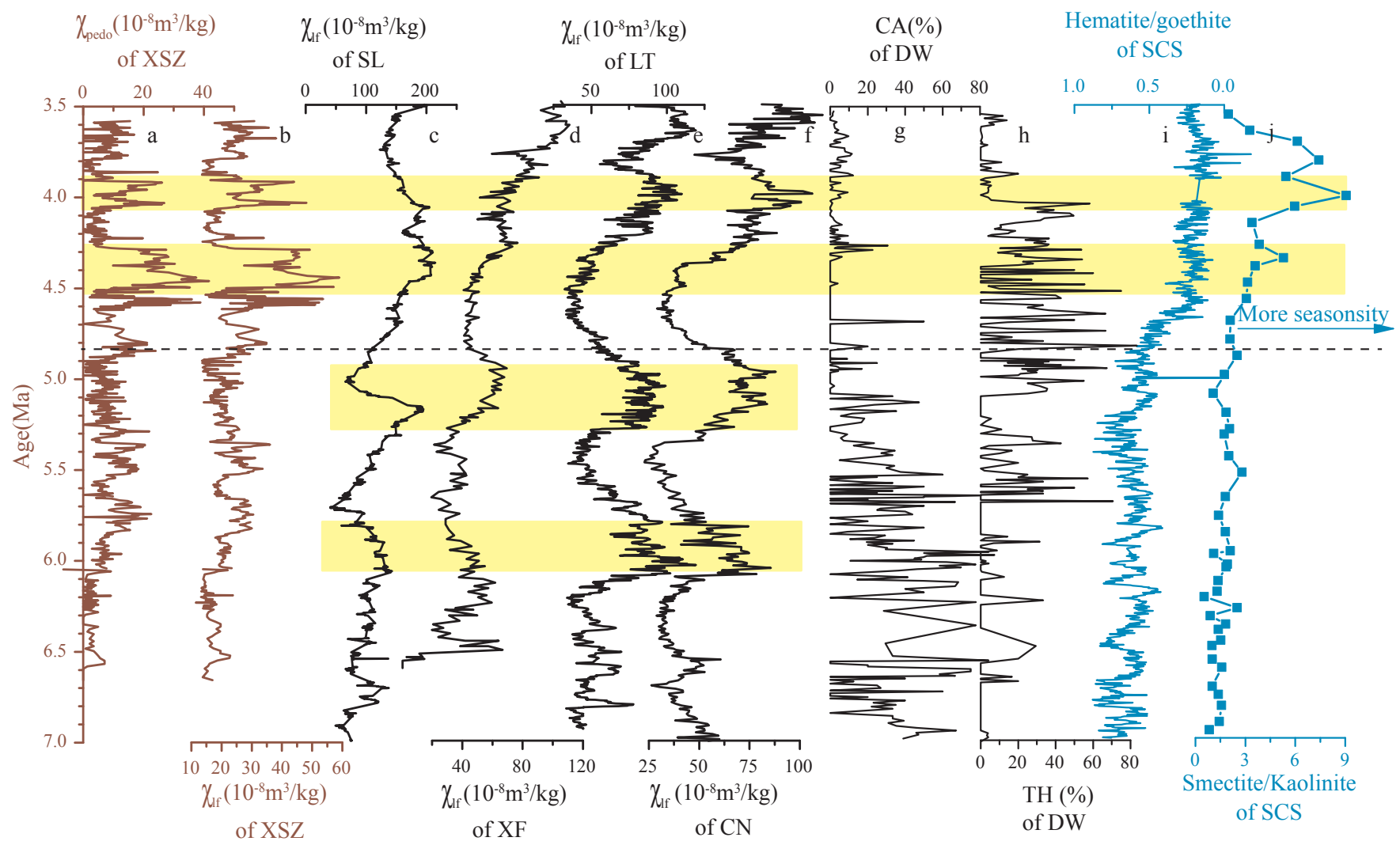


Fig. 7. Comparison of late Miocene-Pliocene paleoclimatic records from Asia. (a-b)  $\chi_{\text{pedo}}$  and  $\chi_{\text{if}}$  from the XSZ section. (c-f)  $\chi_{\text{if}}$  record from Shilou (Ao et al., 2016), Xifeng (Guo et al., 2001), Lingtai (Sun et al., 2010) and Chaona (Song et al., 2007). (g-h) Percentages of cold-aridiphilous (CA) mollusk group and thermo-humidiphilous (TH) mollusk group from Donwan (Li et al., 2008), (i) Hematite/goethite ratio from the South China Sea (Clift, 2006). (j) Smectite/Kaolinite ratio from the South China Sea (Wan et al., 2010; Clift et al., 2014).

Table. 1. The average value and coefficient of variation of the records during two periods of 6.7-4.8 Ma and 4.8-3.6 Ma.

		SiO <sub>2</sub> (%)	Al <sub>2</sub> O <sub>3</sub> (%)	CaO(%)	Fe <sub>2</sub> O <sub>3</sub> (%)	K <sub>2</sub> O(%)
4.8-3.6 Ma	Average	48.9	13.2	11.6	5.69	3
	CV	14.6	9.58	45.57	9.3	12.3
6.7-4.8 Ma	Average	49.5	12.2	11.2	5.2	2.6
	CV	11.6	9.09	32.18	9.6	10.3
		Na <sub>2</sub> O(%)	MgO(%)	Sr(ppm)	Rb(ppm)	Ba(ppm)
4.8-3.6 Ma	Average	1.23	2.3	214.6	109.9	558
	CV	24.4	9	12.5	10.9	11.5
6.7-4.8 Ma	Average	1.2	3.1	211.7	103.9	494
	CV	10.2	61	10.04	10.8	13.2
		CaCO <sub>3</sub> (%)	χ <sub>nf</sub>	χ <sub>lf</sub>	χ <sub>fd</sub>	
4.8-3.6 Ma	Average	13.8	25.4	26.9	1.2	
	CV	45.6	38.3	36.2	78.2	
6.7-4.8 Ma	Average	17.4	19.4	20.3	1	
	CV	29.3	23.8	21.2	72.8	

Table. 2. The correlation coefficient between elements and CaO,

	CaCO <sub>3</sub> and K <sub>2</sub> O		
	CaO	CaCO <sub>3</sub>	K <sub>2</sub> O
Fe <sub>2</sub> O <sub>3</sub>	-0.63	-0.18	-0.29
SiO <sub>2</sub>	-0.95	-0.39	0.72
Al <sub>2</sub> O <sub>3</sub>	-0.77	-0.61	0.95
CaO	1	0.51	-0.67
MgO	-0.04	0.13	-0.11
Na <sub>2</sub> O	-0.06	-0.10	-0.38
K <sub>2</sub> O	-0.67	-0.47	1
Rb	-0.20	-0.36	0.12
Sr	0.24	0.34	-0.29
Ba	-0.25	-0.33	0.63
CaCO <sub>3</sub>	0.51	1	-0.47

Table. 3. The average value and coefficient of variation of the proxies during two periods of 6.7-4.8 Ma and 4.8-3.6 Ma.

		CaCO <sub>3</sub>	Rb/Sr	K <sub>2</sub> O/Na <sub>2</sub> O	$\chi_{lf}$	$\chi_{pedo}$	<2um/>43um
4.8 -3.6	Average	13.8	0.52	2.49	26.9	10.9	1.33
Ma	CV	45.59	23.1	19.4	36.17	78.24	55.7
6.7-4.8	Average	17.4	0.5	2.35	20.3	9.1	1.52
Ma	CV	29.31	14.6	21.3	21.93	72.79	47.55